Int. J. Nano Dimens. 2026; 17(3) : 306-324

International Journal of Nano Dimension (IJND)

https://doi.org/10.57647/ijnd.2026.1703.04

Original Research

Alkali and Alkaline Earth Metal-Centered $B_{12}N_{12}$ Nanocages: A Theoretical Study on the Possibility of Their Application for the Removal of Mefenamic Acid from Aqueous Media

Mousa Soleymani[1,2,*], Mahdieh Rashnooyani[1], Mahdieh Goudarzi[1]

[1]*Department of Chemistry, Faculty of Basic Sciences, Ayatollah Boroujerdi University, Boroujerd, Iran*
[2]*Biosensor and Energy Research Center, Ayatollah Boroujerdi University, Boroujerd, Iran*

[*]**Corresponding author:** m.soleymani@abru.ac.ir

Article History

Received:
10 September 2025
Revised:
8 October 2025
Accepted:
14 October 2025
Published online:
2 January 2026
Published in Issue:
10 July 2026

Abstract:

Pharmaceutical pollutants in water resources are considered as a significant threat to environmental safety and human health. This work addresses this challenge by studying the adsorption of mefenamic acid (MFA) onto the pristine, and alkali and alkaline earth metal ions-centered $B_{12}N_{12}$ nanocage. The most favorable adsorption of MFA on the $B_{12}N_{12}$ nanocage takes place between the boron atom and the oxygen atom of the carboxyl group in MFA. For the nanocage centered with alkali and alkaline earth metal ions, the best results were obtained when the Be^{2+} and K^+ ions are located at the center of the nanocage, in charged and neutralized forms, respectively. Among all nanocages studied in this work, $K^+@B_{12}N_{12}Cl^-$ nanocage showed best performance in the aqueous media. The IGMH and NCI analyses confirmed strong interactions between the adsorbent and MFA in all cases. Moreover, ELF analysis revealed that a single bond forms between the drug and the nanocage, supporting the chemical nature of the adsorption. In fact, while pristine boron nitride nanocages ($B_{12}N_{12}$) can be potentially applied for drug delivery, their adsorption capacity is moderate. This study demonstrates a unique success: The encapsulation of $B_{12}N_{12}$ with Be^{2+} and specially K^+ ions significantly enhances its adsorption capacity.

Keywords: ELF; Encapsulation; IGMH; Metal-centered nanocage; Pharmaceutical pollutant

Cite this article: Soleymani S, Rashnooyani M, Goudarzi M. Alkali and Alkaline Earth Metal-Centered $B_{12}N_{12}$ Nanocages: A Theoretical Study on the Possibility of Their Application for the Removal of Mefenamic Acid from Aqueous Media. Int. J. Nano Dimens. 2026;17(3): 306-324. https://doi.org/10.57647/ijnd.2026.1703.04

1. Introduction

Specific pharmaceutical agents, including various antibiotics, steroid hormones, blood-lipid regulators, and anti-inflammatory drugs, are now recognized as significant emerging pollutants. This is mainly due to their low biodegradability and persistent nature in the environment. These polutants primarily enter wastewater systems from domestic, industrial, medical, aquaculture, and livestock sources, often as unused medications or via urinary and fecal excretion. Their presence causes serious ecological risks to natural ecosystems. Additionally, the inherent diversity and variability of these emerging contaminants present substantial challenges for the accurate analysis and effective monitoring of surface water, groundwater, and wastewater quality on a global scale [1, 2, 3].

Mefenamic acid (MFA) is a nonsteroidal anti-inflammatory drug used as an analgesic agent in the treatment of primary dysmenorrhea [4]. The presence of this drug in both wastewater effluents and surface waters has been reported in many countries [5]. It has been identified in effluents at concentrations exceeding 0.43 ppm [6]. Studies indicate that this drug remains stable in effluents even after wastewater treatment [7].

Carbon-containing nanomaterials show a range of

unique electronic properties, acting as either semiconductors or adsorbent [8, 9, 10]. However, since the discovery of carbon fullerenes, extensive efforts have been made to synthesize fullerene-like structures using non-carbon elements due to their distinct physical and chemical characteristics. In recent years, the properties of nanostructures such as nanowires, nanotubes, and nanocages have garnered significant research interest in applications such as adsorption, drug delivery, and gas storage [11, 12, 13, 14, 15, 16]. Theoretical studies on nanocages of the type $(XY)_n$, where X and Y are elements from groups IIIA and VA of the periodic table, have shown that these nanocages possess narrow band gaps and exhibit greater chemical stability than their carbon-based analogs. Nanocages such as $X_{12}Y_{12}$, $X_{16}Y_{16}$, $X_{24}Y_{24}$, and $X_{28}Y_{28}$ are of particular importance due to their high semiconductor properties. These nanocages with variable sizes have been the subject of numerous theoretical studies aimed at determining their properties [17, 18, 19].

In recent decades, nanostructures have been effectively applied in removing various pollutants from ecosystems. For example, carbon nanotubes (CNTs) have been widely studied as adsorbents for removing environmental contaminants due to their unique properties. However, CNTs face several challenges, such as high toxicity, low hydrophobicity, and a lack of long-term stability. In recent years, boron nitride compounds have emerged as promising tools for adsorbing pollutants from aqueous solutions due to their high oxidation resistance and thermal stability. Moreover, boron nitride materials are non-toxic and more biocompatible than CNTs for wastewater treatment [20, 21, 22].

Boron nitride nanocages exhibit remarkable chemical and physical properties, particularly due to their semiconductor characteristics. Because of the polar nature of B-N bonds, the $B_{12}N_{12}$ nanocage is predicted to be more reactive than the C_{24} cage. For instance, theoretical studies suggest that the $B_{12}N_{12}$ nanocage can store H_2 molecules more efficiently than the C_{24} nanocage. It has been shown that the $B_{12}N_{12}$ nanocage could be a strong candidate for hydrogen adsorption on its surface [23]. Due to the favorable chemical and physical properties of boron nitrides, these nanostructures have diverse potential applications [21, 24, 25, 26, 27].

Comprehensive control over the properties of $B_{12}N_{12}$ nanocages facilitates their various applications. For example, doping with atoms like Mn or Fe, significantly alters the electronic properties of the $B_{12}N_{12}$ nanocage [28]. Fullerene-like BN nanocages are widely used in structural and electronic materials due to their high-temperature stability, Low dielectric constant, high thermal conductivity, and oxidation resistance. Numerous theoretical calculations have explored the interaction of transition metal atoms with BN nanostructures. A work has investigated the adsorption mechanisms of transition metals with $B_{12}N_{12}$ nanocages using density functional theory (DFT) at the B3LYP and M05 levels [29]. Comprehensive analysis of the first-row transition metals adsorbed on fullerene-like $B_{12}N_{12}$ clusters has been reported [30]. In another research, DFT calculations have been examined the adsorption of alkaline earth cations (e.g., Be^{2+}, Mg^{2+}, Ca^{2+}) inside and outside the $B_{12}N_{12}$ cage [31]. Also, studies on H_2 adsorption onto pristine $B_{12}N_{12}$ and alkalinen earth metal-centered (Be, Mg, Ca) nanocages via DFT [32], efficient adsorption of D.D.T. using transition-metal-centered $B_{12}N_{12}$ clusters (Zn, Cu, Ni, Co, Fe) [33], ciprofloxacin removal from aqueous environments using $B_{12}N_{12}$ [34], interaction of the anticancer drug chloromethane with X_3O-$B_{12}N_{12}$ (X = Li, Na, K) [35], H_2 adsorption on pristine and alkali-metal-doped (Li, Na, K) $B_{12}N_{12}$ [36], and the interaction of antidiabetic drug metformin's with alkali metal- centered (Li, Na, K) $B_{12}N_{12}$ [37], have been reported in this regard.

From a practical application point of view, the synthesis feasibility of pristine $B_{12}N_{12}$ nanocages has been demonstrated through the arc-melting method and detected by LD-TOF mass spectrometry [38]. However, the encapsulation of these nanocages with metal ions in order to create stable metal-centered structures remains a significant synthetic challenge, recently explored primarily via theoretical models rather than experimental routes [21, 39]. While biogenic synthesis approaches using plant extracts or micoorganisms offer promising green alternatives for sustainable nanoparticle production, scaling these methods for industrial wastewater treatment have substantial hurdles [40, 41]. These include high energy costs, potential toxicity concerns (particularly for beryllium-based nanocages), and stability issues in wastewater containing competing ions and organic matter [41, 42]. Future studies must focus on developing scalable, eco-friendly synthesis protocols to fill the gap between theoretical predictions and practical applications for pollutant removal [41, 43].

While the potential of BN nanocages for adsorption has been established through prior investigations into specific pollutant classes (e.g., gases [23, 32, 36], pesticides and herbicides [21, 33], or pharmaceuticals such as ciprofloxacin [34] and metformin [37]), a systematic evaluation of mefenamic acid (a prevalent and persistent anti-inflammatory agent) adsorption on both pristine and metal-centered (encapsulated with alkali and alkaline earth metals ions) BN nanocages remains unexplored. Building upon foundational theoretical studies on nanostructures [13, 14, 16, 44, 45, 46, 47], this work extends previous works by specifically targeting mefenamic acid removal. Therefore, considering the importance of the removal of pharmaceutical contaminants from water resources, as well as the significance of theoretical predictions complementing experimental research, this study aims to fill this gap by investigating the potential of both pristine $B_{12}N_{12}$ nanocage and its metal-ion-centered nanocages containing alkali metal ions (Li^+, Na^+, K^+) and alkaline earth metal ions (Be^{2+}, Mg^{2+}, Ca^{2+}) under both charged and neutral conditions. The primary objectives include examining the effects of these metal ions and chloride counterions on the adsorption

https://doi.org/10.57647/ijnd.2026.1703.04

process. To achieve these goals, various analytical tools will be employed, including adsorption energy calculations, charge analysis, Independent Gradient Model based on Hirshfeld partition (IGMH), Non-Covalent Interactions (NCI) and Electron Localization Function (ELF) analyses, establishing key design principles for developing high-efficiency nanocages for the adsorption of pollutants.

2. Materials and methods

Optimization of the geometries was performed using the M062X functional with the 6-311G(d,p) basis set [48]. Frequency calculations were carried out at the same computational level on the optimized structures to determine thermodynamic parameters and to verify the nature of the stationary points. The results confirmed that all structures exhibited no imaginary frequencies. The neutral and charged complexes were optimized at their respective ground-state charge and spin multiplicity settings (0/1 for the neutral and cation charge/1 for the charged species).

For atomic charge analysis, Natural Population Analysis (NPA) was carried out [49].

All calculations were performed using Gaussian 09 software [50], with solvent effects (water) simulated via the Polarizable Continuum Model (PCM) of Tomasi and coworkers [51] within the Self-Consistent Reaction Field (SCRF) framework [52]. For this purpose, the gas-phase optimized geometries were further fully re-optimized in the water as solvent. The Multiwfn software was utilized for IGMH and ELF analyses [53].

The adsorption energy (E_{ads}), enthalpy (ΔH), Gibbs free energy (ΔG), and entropy (ΔS) were derived from the energy difference between the complex and the isolated drug/nanocage components, using equations (1)-(4):

$$E_{ads} = E_{cmpx} - (E_{nanocage} + E_{MFA}) \quad (1)$$

$$\Delta S_{ads} = S_{cmpx} - (S_{nanocage} + S_{MFA}) \quad (2)$$

$$\Delta G_{ads} = G_{cmpx} - (G_{nanocage} + G_{MFA}) \quad (3)$$

$$\Delta H_{ads} = H_{cmpx} - (H_{nanocage} + H_{MFA}) \quad (4)$$

where cmpx, nanocage, and MFA are the abbreviations for complex, nanocage, and mefenamic acid, respectively.

3. Results and discussion

3.1 Investigation of the adsorption of MFA on both pristine $B_{12}N_{12}$ nanocages and metal-centered nanocages

To study the adsorption of mefenamic acid on the $B_{12}N_{12}$ nanocage and the metal-centered nanocage, different adsorption configurations from various sites were investigated. The structures were designed to cover nearly all possible configurations. Thus, ten adsorption situations were examined for adsorption on the $B_{12}N_{12}$ nanocage, and six ones were studied for adsorption on the metal-centered nanocage with alkali (Li^+, Na^+, K^+) and alkaline earth (Be^{2+}, Mg^{2+}, Ca^{2+}) metal ions. Among the studied structures, the configuration with the most negative energy changes, the most favorable adsorption, was selected for further analysis. Then, thermodynamic parameters such as enthalpy, Gibbs free energy, and entropy, have been calculated using the M062X method and 6-311G(d, p) basis set for all configurations at 298.15 K. The results for the most favorable adsorption mode in both gas and solution phases are presented in Table 1. In contrast, those for the other adsorption situations are summarized in Tables S1 and S2 in the supplementary information.

The thermodynamic data summarized in Tables 1, S1, and S2 consistently confirm the spontaneous and exothermic adsorption of MFA onto the $B_{12}N_{12}$ nanocages. The uniformly negative values for both adsorption energy (E_{ads}) and enthalpy change (ΔH) across all configurations in gas and aqueous phases confirm the highly exothermic character of the process.

A key thermodynamic contrast is observed in the gas phase for situations 4, 7, 8, and 9 (Table S1): despite favorable negative enthalpy changes (ΔH), their Gibbs free energy (ΔG) is positive. This indicates that although the adsorption itself is exothermic, the process is entropically disfavored, likely due to a significant loss of freedom of the drug molecule upon binding to the nanocage surface. The unfavorable entropy is large enough to overcome the favorable enthalpy term, resulting in these processes being non-spontaneous under standard conditions.

Among all configurations, the adsorption situation detailed in Table 1 emerges as the most thermodynamically favorable, displaying remarkable energetics with E_{ads} = −137.54 kJ/mol and a negative ΔG of −78.34 kJ/mol. This combination confirms not only a significant energy release upon adsorption but also a strong driving force for spontaneity, resulting from a balance where the favorable ΔH outweighs any entropic costs ΔS.

The transition to the aqueous phase introduces critical solvent stabilization effects that modify the adsorption process. Geometries 4, 7, and 8 show a positive ΔG, confirming their non-spontaneity is resulted from entropic factors that outweigh the exothermic enthalpy. This suggests that the solvation is insufficient to compensate for the unfavorable entropy associated with these adsorption situations.

Once again, the geometry in Table 1 exhibites superior performance in the solution phase. It shows the highest energy release (E_{ads} = −122.43 kJ/mol) and a strongly negative Gibbs free energy (ΔG = −62.39 kJ/mol). The decrease in the absolute values of E_{ads} and ΔG in solution relative to the gas phase is expected. It arises from the stabilization of the free drug and nanocage by the polar solvent, which reduces the net energetic benefit of adsorption. Nevertheless, the large negative ΔG makes this configuration stable in an aqueous environment, an advantage for its potential use as a drug delivery system. This detailed thermodynamic comparison across phases provides deep insight into the interplay of enthalpy, entropy, and solvation in determining the adsorption process.

Table 1. Thermodynamic parameters for the most favorable adsorption configuration of mefenamic acid (MFA) on $B_{12}N_{12}$ nanocages in both gas and aqueous phases.

Phase	Optimized geometry	ΔG (kJ/mol)	ΔH (kJ/mol)	ΔS (kJ/K·mol)	E_{ads} (kJ/mol)
Gas	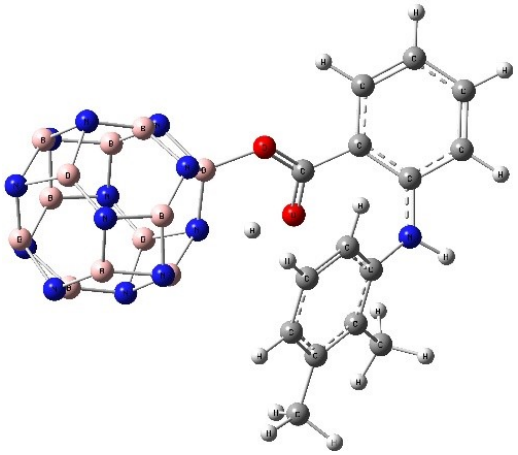	−78.34	−140.04	−0.207	−137.54
Water	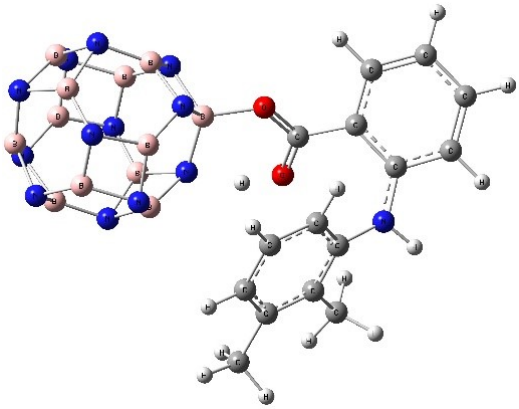	−62.39	−122.42	−0.202	−122.43

Building upon the optimal adsorption configuration identified in Table 1, we systematically investigated the effects of encapsulating alkali and alkaline earth metal ions within the nanocage center. Following structural optimization, thermodynamic parameters for drug adsorption were recalculated. The most favorable results for the $Be^{2+}@B_{12}N_{12}$ system are presented in Table 2. At the same time, complete datasets for other metal ions (Li^+, Na^+, K^+, Mg^{2+} and Ca^{2+}) are provided in Tables S3 and S4 of ESI, covering both gas and aqueous phases.

An analysis of the adsorption energies establishes the beryllium-centered nanocage ($Be^{2+}@B_{12}N_{12}$) as an excellent adsorbent for MFA. This system exhibits unique thermodynamic parameters that underscore its remarkable binding affinity, characterized by an adsorption energy of −526.19 kJ/mol, an enthalpy change (ΔH) of −509.64 kJ/mol, and a Gibbs free energy change (ΔG) of −458.33 kJ/mol. These values collectively demonstrate a highly exothermic and spontaneous adsorption process, indicating both a significant energy release and a strong thermodynamic driving force favoring complex formation. The magnitude of these values clearly indicates a chemisorption process. This strong binding originates from a Lewis acid-base interaction between the hard acid Be^{2+} center and the oxygen atom of carboxyl group of MFA as a hard base. From an application perspective, such high exothermicity and spontaneity are highly desirable for the irreversible isolation and complete removal of the pollutant from water sources. However, the strength of adsorption may create a challenge for adsorbent regeneration, suggesting that the $Be^{2+}@B_{12}N_{12}$ nanocage is ideally suitable for single-use applications in purifying water to very low contamination levels, rather than for multiple cycles of reuse.

Notably, all examined adsorption configurations (including those on pristine $B_{12}N_{12}$ and other metal-centered nanocages) consistently exhibit negative entropy changes (ΔS). This universal observation reflects a substantial reduction in the degrees of freedom of both the drug molecule and the nanocage upon adsorption, resulting in increased molecular arrangement during the process.

Under aqueous phase conditions, the $Be^{2+}@B_{12}N_{12}$ complex shows its good performance as adsorbent, even

Table 2. Thermodynamic parameters for mefenamic acid adsorption on $Be^{2+}@B_{12}N_{12}$ nanocages in gas and aqueous phases.

Phase	Optimized geometry	ΔG (kJ/mol)	ΔH (kJ/mol)	ΔS (kJ/K·mol)	E_{ads} (kJ/mol)
Gas	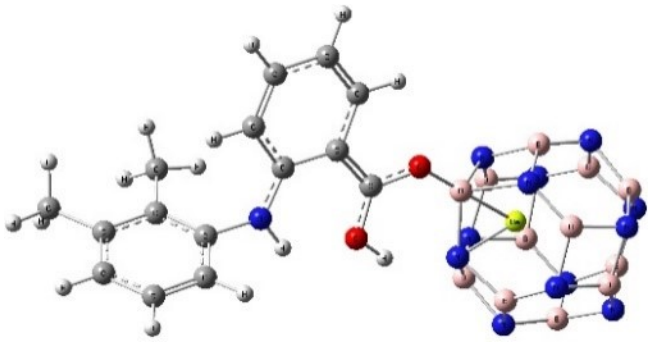	−458.33	−509.64	−0.172	−526.19
Water	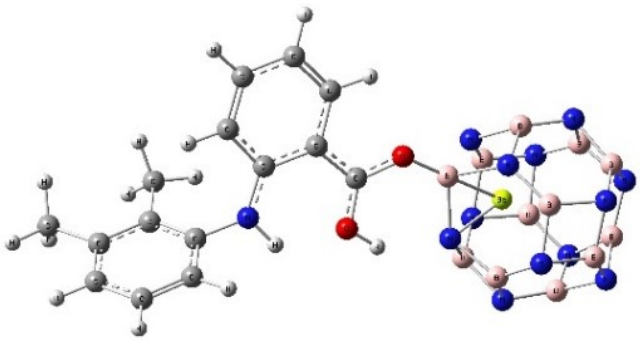	−273.51	−329.39	−0.188	−337.13

though their energetics is attenuated by solvation effects. The values shift to −337.13 kJ/mol (E_{ads}), −329.39 kJ/mol (ΔH), and −273.51 kJ/mol (ΔG). This attenuation is expected, as the polar solvent molecules stabilize both the free drug and nanocage, thereby reducing the net energetic benefit of adsorption. Nevertheless, the maintained strongly negative values confirm the stability of this adsorption system in aqueous media.

The exceptional adsorption capacity of the beryllium-centered system can be primarily attributed to the unique combination of the Be^{2+} with a small ionic radius and exceptionally high charge density, which enables strong electrostatic interactions and potentially partial covalent character in bonding with the oxygen atom of the carboxyl group of MFA.

An important comparative outcome from this study is that the drug adsorption occurs consistently more effectively on metal-centered nanocages compared to the pristine $B_{12}N_{12}$ structure. This demonstrates conclusively that encapsulating the $B_{12}N_{12}$ nanocage with metal ions significantly enhances interaction energies through improved electrostatic forces, leading to stronger and more favorable adsorption processes.

In the next step, to investigate the effect of system neutrality, adsorption was studied in both gaseous and solution phases by adding chloride ions corresponding to the cation's charge. In other words, a neutral nanocage/salt structure was considered as the adsorbent, and thermodynamic parameters were calculated. The role of the chloride ion is not to act as an adsorption site but to serve two critical purposes:

1. Charge neutrality: It causes the overall complex remains electrically neutral, balancing the positive charge of the encapsulated metal ions.

2. Electronic engineering: The metals ions and Cl^- ions work in tandem to create an intense internal dipole moment. This polarizes the electron density of the $B_{12}N_{12}$ cage itself, making its surface more electrostatically active and enhancing its affinity for MFA. The adsorption occurs on the surface atoms of the polarized nanocage, not directly on the Cl^- ion.

The results for the most favorable case ($K^+@B_{12}N_{12}Cl^-$) are presented in Table 3, while those for other cases are provided in Tables S5 and S6.

A comprehensive analysis of the adsorption energies exhibites are striking differences between various nanocage systems. According to the results presented in Tables 3, S5, and S6, the $K^+@B_{12}N_{12}Cl^-$ nanocage demonstrates the best performance, achieving the highest adsorption energy values among all systems investigated: −513.15 kJ/mol in the gaseous phase and −425.24 kJ/mol in the solution phase. This system also shows remarkably favorable Gibbs free energy values of −434.50 kJ/mol (gas phase) and −343.02 kJ/mol (solution phase), indicating a highly spontaneous and thermodynamically

Table 3. Thermodynamic parameter values for the adsorption of mefenamic acid drug molecules on the $K^+@B_{12}N_{12}Cl^-$ nanocage in gaseous and solution phases.

Phase	Optimized geometry	ΔG (kJ/mol)	ΔH (kJ/mol)	ΔS (kJ/K·mol)	E_{ads} (kJ/mol)
Gas	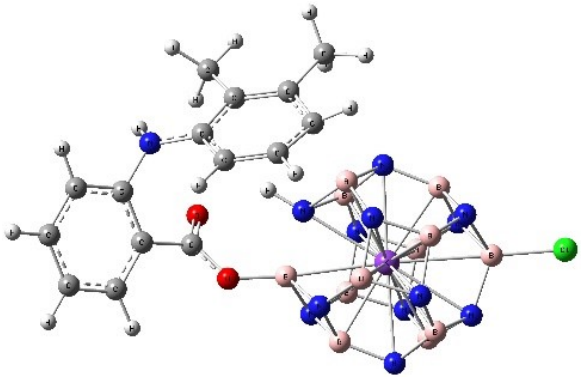	−434.50	−507.92	−0.247	−513.15
Water	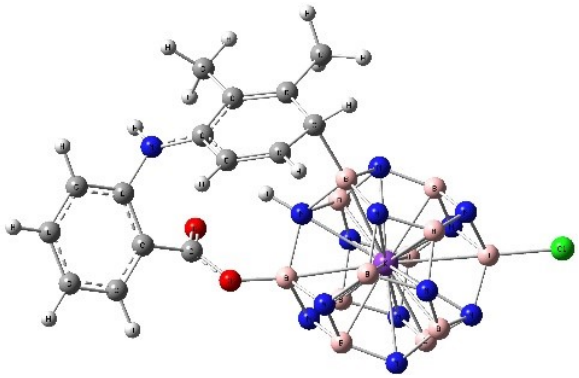	−343.02	−425.19	−0.276	−425.24

favorable adsorption process.

The excellent performance of the $K^+@B_{12}N_{12}Cl^-$ nanocage can be attributed to its unique electronic structure and charge distribution. The incorporation of both K^+ and Cl^- ions creates a balanced charge environment that facilitates strong electrostatic interactions with MFA's functional groups. The neutral character of this nanocage enhances its stability in both gaseous and aqueous solution while maintaining strong adsorption capabilities. On the other hand, the $CaCl^{2-}$ based system exhibits fundamentally different thermodynamic behavior. The Gibbs free energy changes for adsorption show positive values in both gaseous and solution phases, clearly indicating that the adsorption process is thermodynamically non-spontaneous for this system. This striking difference highlights the crucial importance of the selected metal ion and nanocage engineering in determining adsorption feasibility.

The suitable performance of the $K^+@B_{12}N_{12}Cl^-$ system, particularly in the solution phase, underscores its potential practical applicability in drug delivery applications where aqueous environments are biologically relevant. The maintenance of strongly negative ΔG values despite solvent effects exhibites the stability of this adsorption system and its promise for pharmaceutical nanocarrier development.

Our analysis confirms that while the pristine $B_{12}N_{12}$ nanocage exhibits remarkable rigidity with minimal structural change upon adsorption, the metal ion-encapsulated nanocages, particularly $Be^{2+}@B_{12}N_{12}$, undergo slight but meaningful structural distortions. These distortions are primarily localized around the metal ion adsorption site. They are a direct consequence of the strong Lewis acid-base interaction and significant charge transfer between the nanocage and the MFA. Importantly, our calculations show that these distortions do not affect the overall stability of the nanocage geometry. The binding energy of the metal ion-encapsulated nanocages remain highly negative, and the distorted structure exhibites a new, stable energy minimum for the adsorption complex, as evidenced by the lack of imaginary frequencies in the vibrational frequency calculations.

Geometric analysis of the MFA–$Be^{2+}@B_{12}N_{12}$ complex exhibites a significant elongation in one of the B-N bonds connected to the boron atom bonded to the oxygen atom of MFA, increasing from 1.450 Å in the pristine $Be^{2+}@B_{12}N_{12}$ nanocage to 1.706 Å upon adsorption. In addition, adsorption of MFA on the $K^+@B_{12}N_{12}Cl^-$ nanocage results in elongation of the B-N bonds linked to the boron atoms interacting with both the oxygen and carbon atoms of MFA, with bond lengths increasing from 1.470 Å to 1.671 Å. These bond elongations

account for the remarkably high adsorption energies observed in our study, confirming that the encapsulated nanocages undergo strong chemisorption rather than physisorption. This mechanism confirms strong and stable binding, highlighting the suitability of these systems for applications requiring robust molecular capture.

To evaluate the validity of our chosen functional (M06-2X/6-311G(d,p) for modeling the adsorption process, a benchmarking study was carried out. The interaction energies for charged complexes were recalculated using the long-range corrected ωB97XD functional with the correlation-consistent cc-pVDZ basis set [54]. The results obtained from both methods are summarized in Table S7 of ESI. As illustrated in figure 1 good agreement is observed between the adsorption energies, enthalpies, and Gibbs free energies obtained from the M06-2X and ωB97XD methods. This excellent agreement validates the reliability of the trends reported in this study. Both computational approaches consistently indicate the MFA-Be^{2+}@$B_{12}N_{12}$ complex as possessing the most favorable adsorption characteristics and the highest stability. Thus, the results obtained by the M06-2X/6-311G(d,p) level of theory are well-founded.

To analysis the potential dependence of our adsorption energetics on the choice of implicit solvation model, a benchmark study was performed on the MFA-Be^{2+}@$B_{12}N_{12}$ complex. The thermodynamic parameters were recalculated using the IEFPCM and SMD models [52, 55], in addition to the default PCM approach. The results presented in Table 2, indicate that the absolute values of ΔG, ΔH and specially E_{ads} and ΔS exhibite only minor variations across the different models. The consistency between the parameters obtained from PCM, IEFPCM, and SMD models, as depicted in figure 2, confirms that the conclusions of this work are robust against the selection of these commonly used solvation models.

The plots demonstrate the strong agreement between the PCM, IEFPCM, and SMD models for the Gibbs free energy, enthalpy and especially for adsorption energy and entropy for the MFA-Be^{2+}@$B_{12}N_{12}$ system. The high degree of agreement highlights the insensitivity of the comparative trends to the chosen solvation model.

3.2 IGMH and NCI analysis on more favorable adsorption configurations

In 2017, the Independent Gradient Model (IGM) was introduced by Henon et al. to study interaction regions [56]. These regions are visualized using isosurfaces of δg and sign(λ_2)ρ, which highlight different types of interactions. In 2022, an improved version called the Hirshfeld-based Independent Gradient Model (IGMH) was developed by Lu and coworkers. Unlike the original IGM, which relies on simplified electron densities, IGMH utilizes atom-weighted Hirshfeld electron densities derived from real molecular electron distributions [57]. This refinement provides a more accurate representation of interactions by incorporating actual molecular electron densities.

For MFA, two possible conformers were considered, differing in the configuration of hydrogen and nitrogen atoms (figure 3). Computational results revealed that the left conformer is 30.80 kJ/mol more stable than the right one. This stability can be attributed to the formation of an intramolecular hydrogen bond. To move

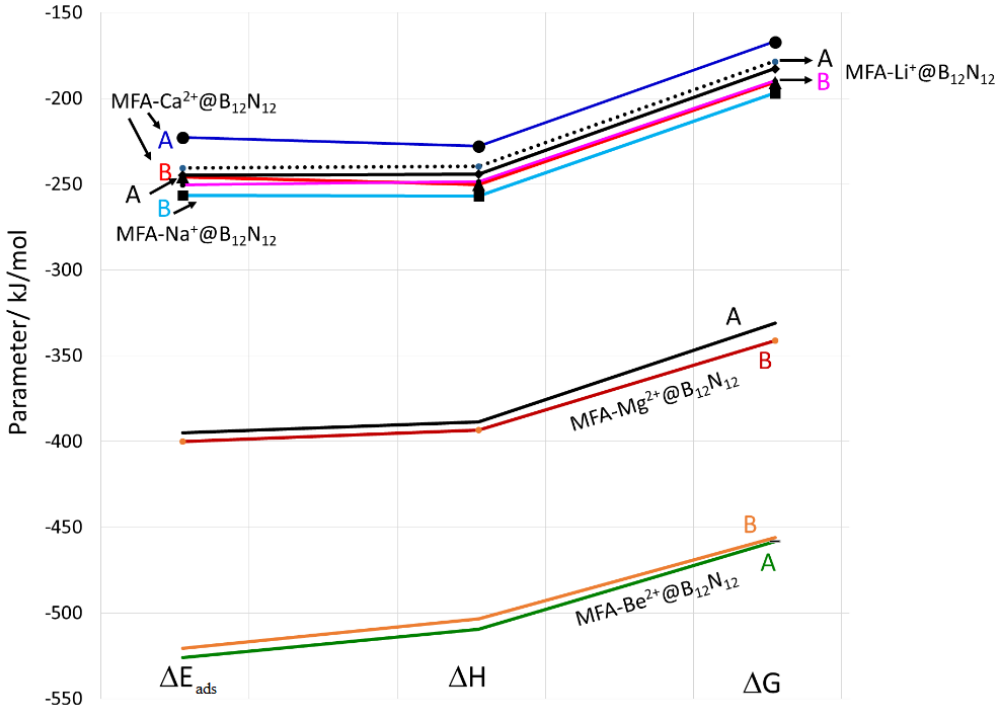

Figure 1. Comparison between the thermodynamic parameters of adsorption obtained from the M06-2X/6-311G(d,p) (A) and ωB97XD/cc-pVDZ (B) methods for the MFA adsorption on metal-ion-centered $B_{12}N_{12}$ nanocages.

https://doi.org/10.57647/ijnd.2026.1703.04

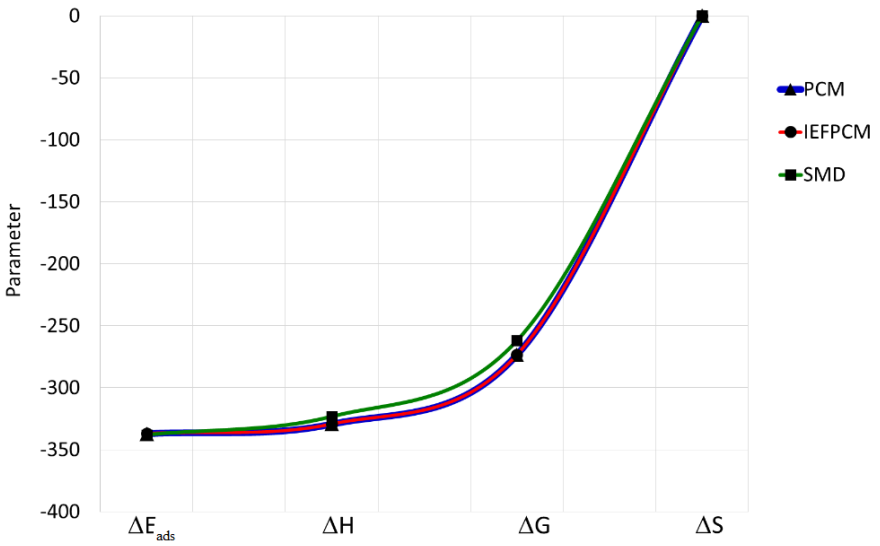

Figure 2. Comparison of thermodynamic parameters obtained from different solvation models.

beyond energy calculations and visually characterize the electronic nature of this stabilizing interaction, we employed the Independent Gradient Model based on Hirshfeld partition (IGMH). The IGMH analysis shows a blue isosurface region between the hydrogen and nitrogen atoms, proving the presence of a hydrogen bond. This advanced topological analysis explains the enhanced stability of the left conformer, which was used for all subsequent calculations.

To gain deeper insight into the adsorption process of MFA on the nanocages, we employed the IGMH topological analysis on the drug-nanocage complexes. This method is particularly valuable as it moves beyond adsorption energies to offer direct visualization and characterization of the non-covalent interactions responsible for adsorption. For each system, the configuration with the most negative adsorption energy (the most stable complex) was selected for IGMH evaluation. The results

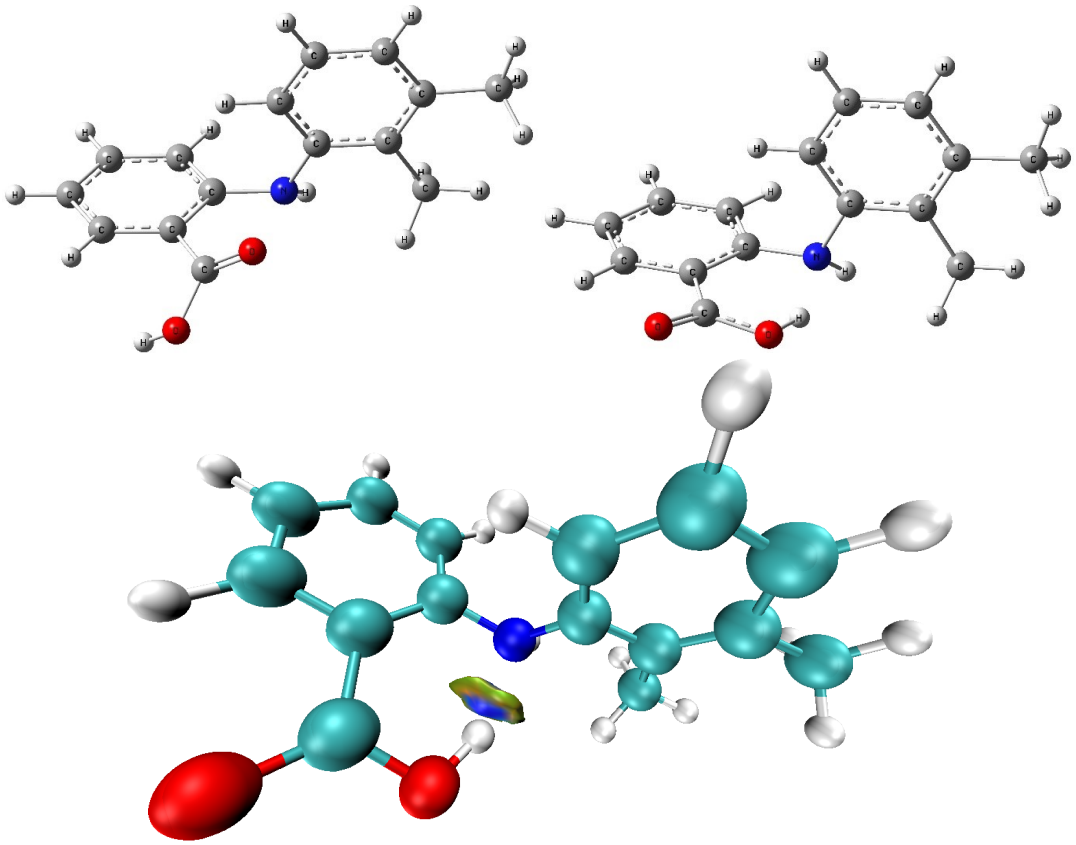

Figure 3. Structures of mefenamic acid (top) and IGMH analysis of the more stable conformer (down).

https://doi.org/10.57647/ijnd.2026.1703.04

are presented in Figs. 4 (a, b, c, d).

The isosurfaces depict the nature and strength of the interactions between MFA and (a) pristine $B_{12}N_{12}$, (b) $Be^{2+}@B_{12}N_{12}$, and (c) $K^{+}@B_{12}N_{12}Cl^{-}$ nanocages. The color coding on the isosurfaces (see scale in d) determines the type of interaction. The extensive blue regions in (b) and (c) provide visual evidence of the strong, specific chemisorption between the drug's carboxylate group and the metal centers, directly correlating with the calculated high adsorption energies. This analysis supports the critical role of metal ion encapsulation in enhancing the adsorbent's performance of the pollutant.

For adsorption on the pristine $B_{12}N_{12}$ nanocage (Fig. 4 (a)), the IGMH analysis clearly visualizes the chemisorption process through the formation of a prominent blue isosurface region between MFA and the nanocage. This blue region is a direct descriptor of strong interactions.

For the Be^{2+}-centered nanocage ($Be^{2+}@B_{12}N_{12}$), the IGMH result in Fig. 4 (b) reveals two types of interactions: a green isosurface, indicative of van der Waals forces, and an adjacent blue isosurface, specifying a stronger interaction.

The analysis of the neutral $K^{+}@B_{12}N_{12}Cl^{-}$ system (Fig. 4 (c)) shows interesting outcomes. The IGMH analysis reveals two interactions: a prominent blue isosurface between the drug's phenyl ring and a boron atom, suggesting a strong, possibly covalent-like interaction, and a strong interaction between the carboxyl oxygen atom and a boron atom. This analysis visually demonstrates how these synergistic interactions collectively contribute to a strong adsorption observed in this system. This ability to determine the nature of interactions in the complexes highlights the critical role of topological analysis in understanding adsorption mechanisms (Fig. 4 (d)).

The electron density gradient (δg_{inter}) versus $sign(\lambda_2)\rho$ plots for the adsorption of mefenamic acid on $B_{12}N_{12}$ (a), $Be^{2+}@B_{12}N_{12}$ (b), and $K^{+}@B_{12}N_{12}Cl^{-}$ (c) nanocages are presented in Fig. 5. The red peaks in Fig. 5 (a) indicate the interaction between the oxygen atoms of the carboxyl group of MFA with the boron atom of $B_{12}N_{12}$ nanocage. Strong interactions between MFA and the $Be^{2+}@B_{12}N_{12}$ as well as $K^{+}@B_{12}N_{12}Cl^{-}$ nanocages are depicted also with red peaks in Figs. 5 (b,c), respectively. Notably, a prominent red peak was observed around $sign(\lambda_2)\rho = -0.040$ a.u. confirms the existence of a strong bond between the carboxyl group's oxygen atom and the boron atom of the nanocage.

Next, Non-Covalent Interaction (NCI) analysis was employed to visualize and characterize the nature of the interactions between MFA and the nanocages. The NCI analysis is based on the electron density and its reduced gradient, allowing for the visualization of weak non-covalent interactions and steric repulsions as distinct isosurfaces [58]. To gain further insight into the nature of the adsorption, NCI analysis was performed on the

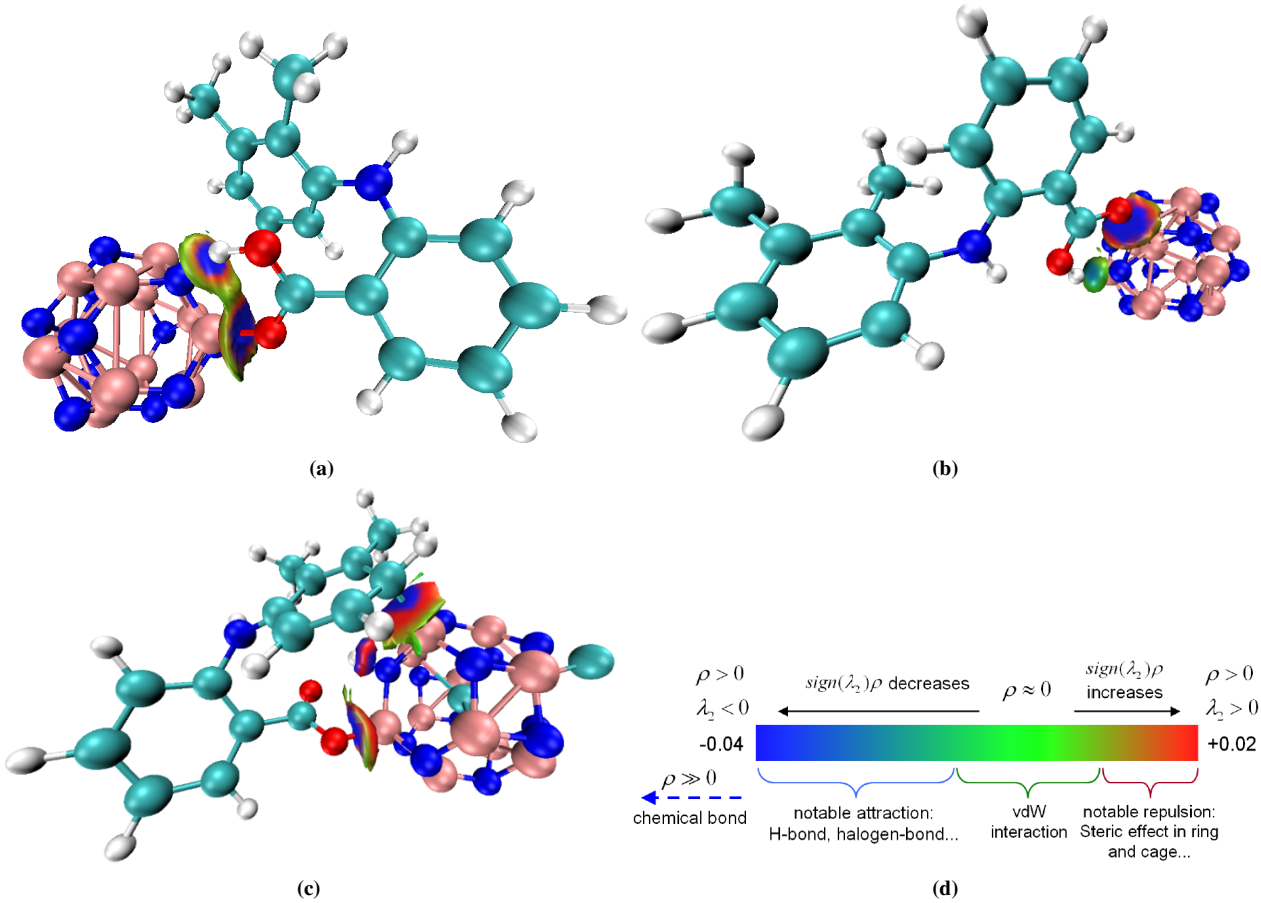

Figure 4. (a, b, c, d). Visualizing non-covalent interactions via IGMH analysis.

https://doi.org/10.57647/ijnd.2026.1703.04

most favorable complexes, and the results are depicted in Fig. 6. The NCI analysis confirms the results obtained by the IGMH and ELF analyses. For the MFA@$B_{12}N_{12}$ complex, the isosurface observed between the aromatic ring of MFA and the nanocage reveals van der Waals interactions. A hydrogen bond is also observed between the acidic hydrogen of MFA and a nitrogen atom of the nanocage. Most significantly, the region between the carboxyl oxygen atom and the boron atom indicates no isosurface associated with weak interactions, which is consistent with the presence of a strong, covalent-like bond as suggested by the adsorption energy and IGMH analysis.

A similar trend is observed for the MFA@Be^{2+}@$B_{12}N_{12}$ complex, where the primary interaction site (the B-O region) is characterized by the absence of weak NCI features, confirming a strong chemisorption process. The NCI plot for the MFA@K^+@$B_{12}N_{12}$ complex primarily reveals van der Waals forces between the aromatic ring of MFA and the nanocage. Again, at the adsorption site (the B-O region), no weak interactions are observed, which is consistent with the chemisorption nature resulted by the adsorption energy and IGMH analysis. The excellent consistency between the adsorption energy, NCI, and IGMH provides a comprehensive and valid picture of the interaction nature in these drug-nanocage systems.

3.3 Calculation of charge transfer (GEDT) and charge transfer analysis on the favorable adsorption situations

The occurrence of adsorption is typically accompanied by electron transfer from one species to another, resulting in attractive forces between them. Figure 7 displays the atomic charge distribution, where atoms appearing closer to green in the color scale represent more positive charges, while those tending toward red indicate more negative charges. For MFA, the charge distribution varies from −0.720 to +0.849, while for the $B_{12}N_{12}$ nanocage it ranges from −1.180 to +1.180. The charge variations for modified nanocages show −1.166 to +1.644 for Be^{2+}@$B_{12}N12_{12}$ and −1.259 to +1.282 for K^+@$B_{12}N_{12}Cl^-$. In the optimized adsorption configurations, the following charge distributions are observed: MFA-$B_{12}N_{12}$ complex: −1.311 to +1.228, MFA-Be^{2+}@$B_{12}N_{12}$ system: −1.318 to +1.692, and MFA-K^+@$B_{12}N_{12}Cl^-$ complex: −1.311 to +1.266. The Natural Population Analysis (NPA) charges for all atoms

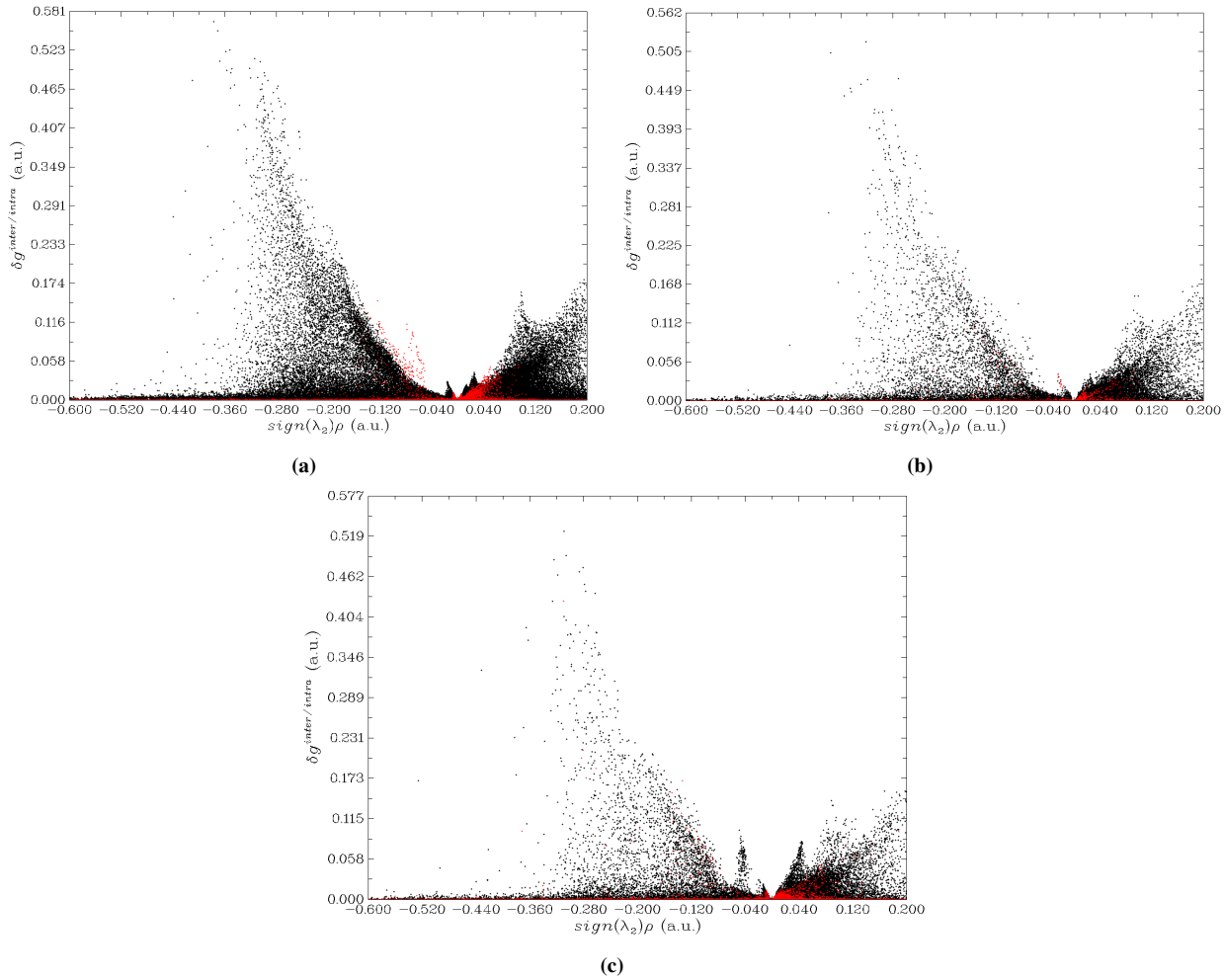

Figure 5. Electron density gradient (δg_{inter}) versus sign(λ_2)ρ plots for the adsorption of mefenamic acid on (a) pristine $B_{12}N_{12}$ nanocage, (b) Be^{2+}@$B_{12}N_{12}$ nanocage, and (c) K^+@$B_{12}N_{12}Cl^-$ nanocage.

https://doi.org/10.57647/ijnd.2026.1703.04

in the isolated systems and the most favorable complexes are also presented in Fig. S1 of ESI.

According to the numeric values of atomic charges depicted in figure 7, all interactions take place between the negatively charged oxygen atom of the carboxyl group and the positively charged boron atom of the nanocage. Furthermore, in all adsorption processes, the positively charged hydrogen of the carboxyl group acts as a bridge, interacting on one side with the nitrogen atom of the nanocage and on the other side with another oxygen atom of the carboxyl group, thereby enhances the adsorption process. Additionally, in the case of MFA adsorption on $KCl@B_{12}N_{12}$ nanocage, an additional bond is formed between the 4-position carbon atom of the phenyl group of MFA, which carries a negative charge, and the boron atom of the nanocage, which exhibites a positive charge. The last interaction improves the adsorption process.

Beyond the theoretical conditions presented here, the practical environmental application of $Be^{2+}@B_{12}N_{12}$ necessitates consideration of complex real-world factors. In natural water sources, the presence of competing ions (e.g., Ca^{2+}, Mg^{2+}, Na^{+}, . . .) could potentially affect the adsorption capacity through competitive binding at the nanocage's active sites. However, the predicted high affinity and selectivity of the Be^{2+} center for the carboxylate group of MFA may reduce this effect. Furthermore, solution pH is a critical parameter because it affects the ionization of MFA (pKa ~ 4.2) and the surface charge of the nanocage. The optimal adsorption probably occurs near neutral to basic pH, where the drug is deprotonated to the carboxylate ion, and the corresponding electrostatic attraction to the cationic Be^{2+} center is increased. Future studies should experimentally validate these predictions in complex mixture, to fully evaluate the nanocage's performance and potential for irreversible sequestration of polutants under environmentally relevant conditions.

Molecular interactions are accompanied by charge transfer, which significantly affects the interaction energy. The degree of charge transfer, known as Global Electron Density Transfer (GEDT), serves as an indicator of electron redistribution between interacting species and the polarity between them [59]. In this regard, the GEDT values were calculated for the most favorable complex of mefenamic acid on both pristine $B_{12}N_{12}$ and the Be^{2+}-centered nanocage ($Be^{2+}@B_{12}N_{12}$). These results, along with the Molecular Electrostatic Potential (MEP) maps, are presented in figure 8. In the MEP maps, blue regions correspond to areas of low electron density (positive electrostatic potential) and red regions represent zones of high electron density (negative electrostatic potential).

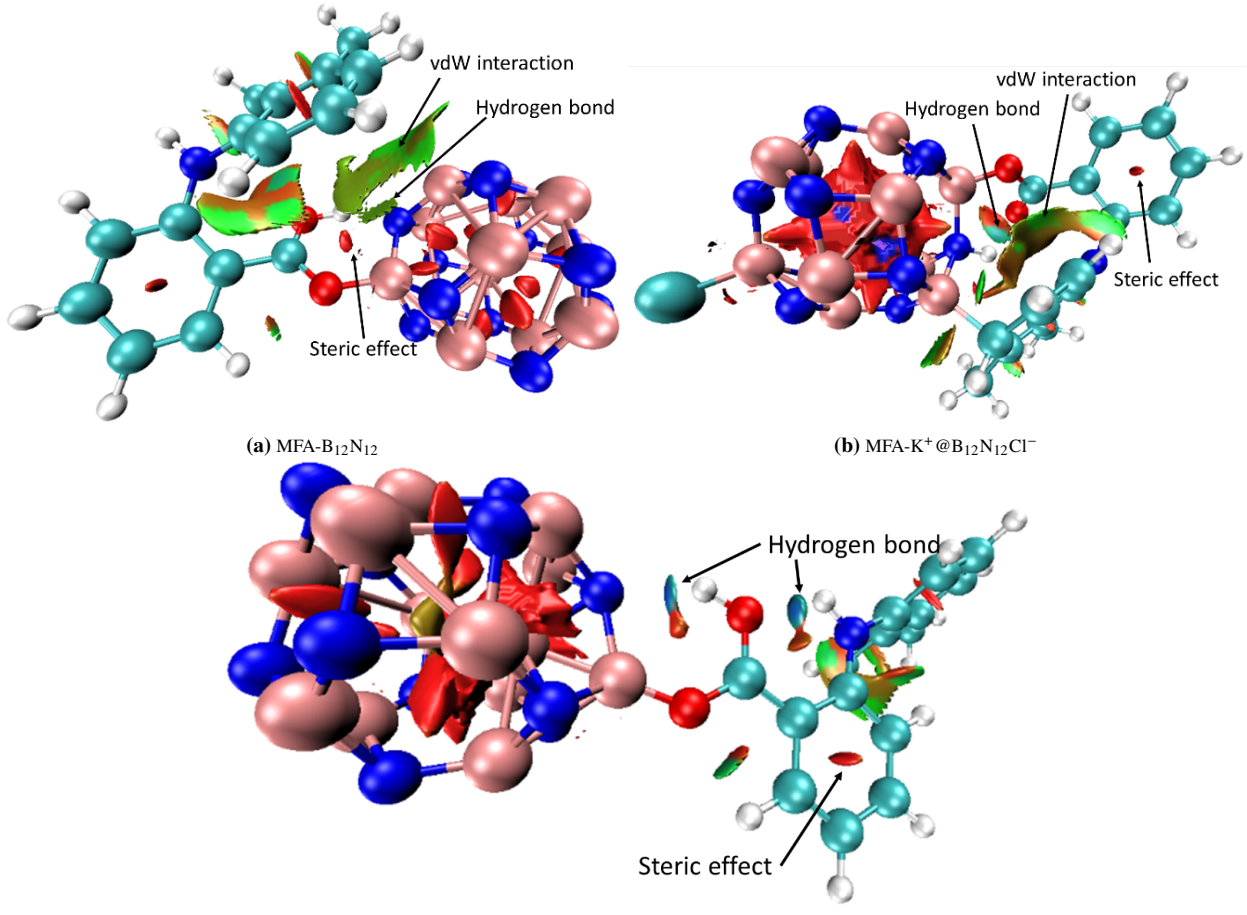

(a) MFA-$B_{12}N_{12}$ **(b)** MFA-$K^{+}@B_{12}N_{12}Cl^{-}$

(c) MFA-$Be^{2+}@B_{12}N_{12}$

Figure 6. Non-covalent interaction (NCI) analysis for the adsorption of MFA on the pristine $B_{12}N_{12}$, $K^{+}@B_{12}N_{12}Cl^{-}$ and $Be^{2+}@B_{12}N_{12}$ nanocages. The green and blue-green surfaces specify van der Waals interactions and hydrogen bonds, respectively. The absence of weak interaction features at the primary adsorption site (The B-O bonding region) confirms a strong chemisorption process.

https://doi.org/10.57647/ijnd.2026.1703.04

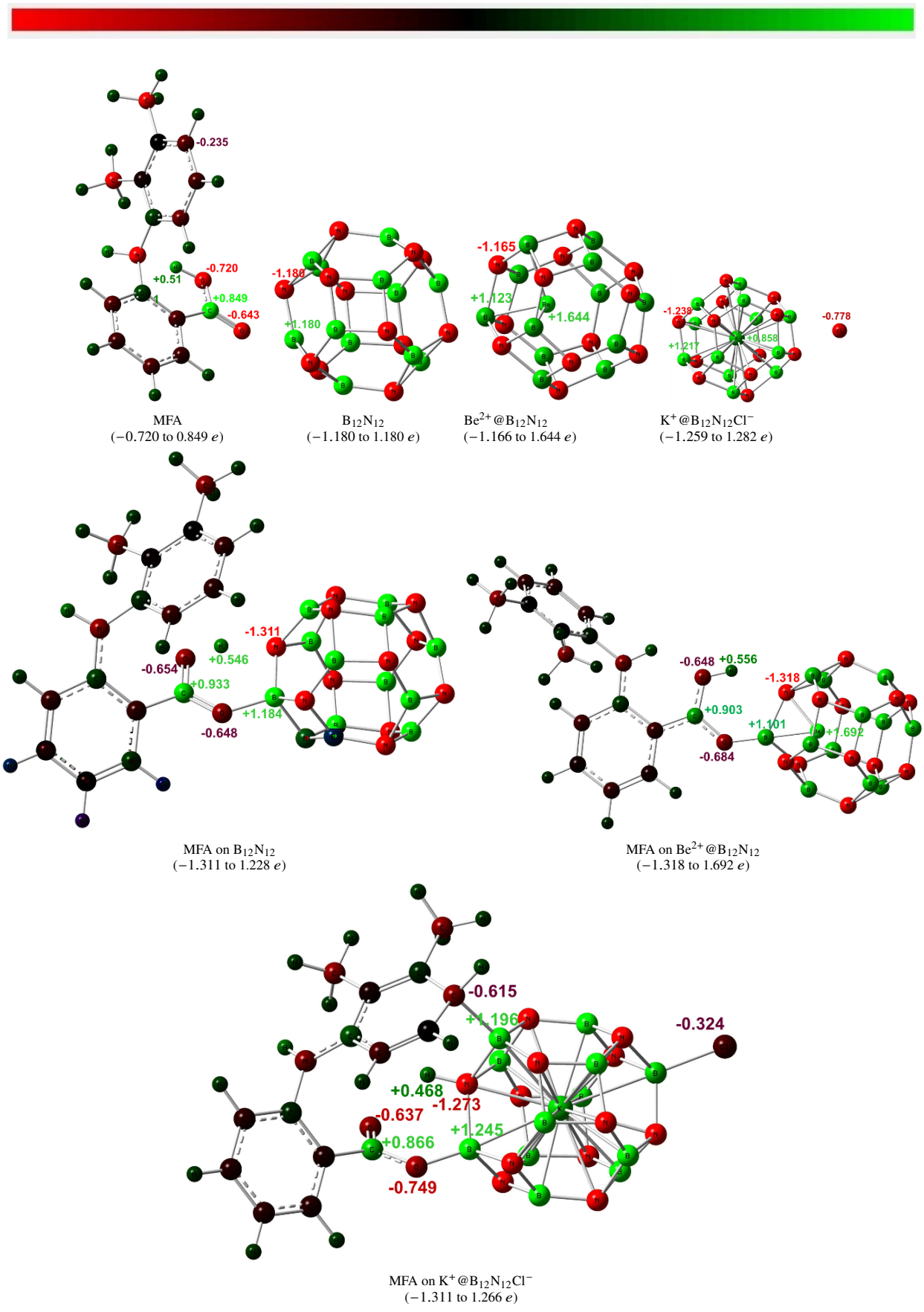

Figure 7. The distribution of NBO atomic charges on the initial structures and the corresponding complexes.

https://doi.org/10.57647/ijnd.2026.1703.04

The analysis of GEDT values and MEP maps reveals crucial insights into the adsorption mechanisms. For the pristine $B_{12}N_{12}$ nanocage, a GEDT value of 0.398 *e* confirms significant electron transfer from MFA toward the nanocage, evidenced by the intense blue region on the drug molecule at the adsorption site. This substantial charge transfer correlates well with the strong adsorption observed in previous thermodynamic analyses. The Be^{2+}-centered nanocage shows even greater electron transfer (0.486 *e*), though the nanocage maintains a net positive charge visible as deep blue regions in the MEP map. This positive potential suggests the metal center enhances the nanocage's electron-accepting power while preserving its cationic character. The drug molecule exhibits pronounced electron depletion (blue regions). In the $K^+@B_{12}N_{12}Cl^-$ system, the MEP shows distinct features in which the chloride ions appear as red regions (electron-rich). At the same time, the nanocage framework exhibites yellow tones indicating moderate electron density. The drug molecule again shows blue regions of electron depletion, with a measured GEDT of 0.287 *e*. This reduced charge transfer compared to the Be^{2+} system reflects the different electronic environment created by the chloride counterions.

3.4 Electron localization function (ELF) analysis

To characterize the nature of the chemical bonding and provide definitive electronic-level evidence for the adsorption mechanism, we performed a topological analysis of the Electron Localization Function (ELF). This advanced quantum-chemical method clearly indicates electron distribution patterns, characterizes regions of electron pairing, and allows for the definitive classification of chemical bond types formed during adsorption. The ELF results provide critical quantitative insights that perfectly confirm the IGMH findings. The results of ELF analysis for the most favorable complexes are given in Figs. 9 (a-f).

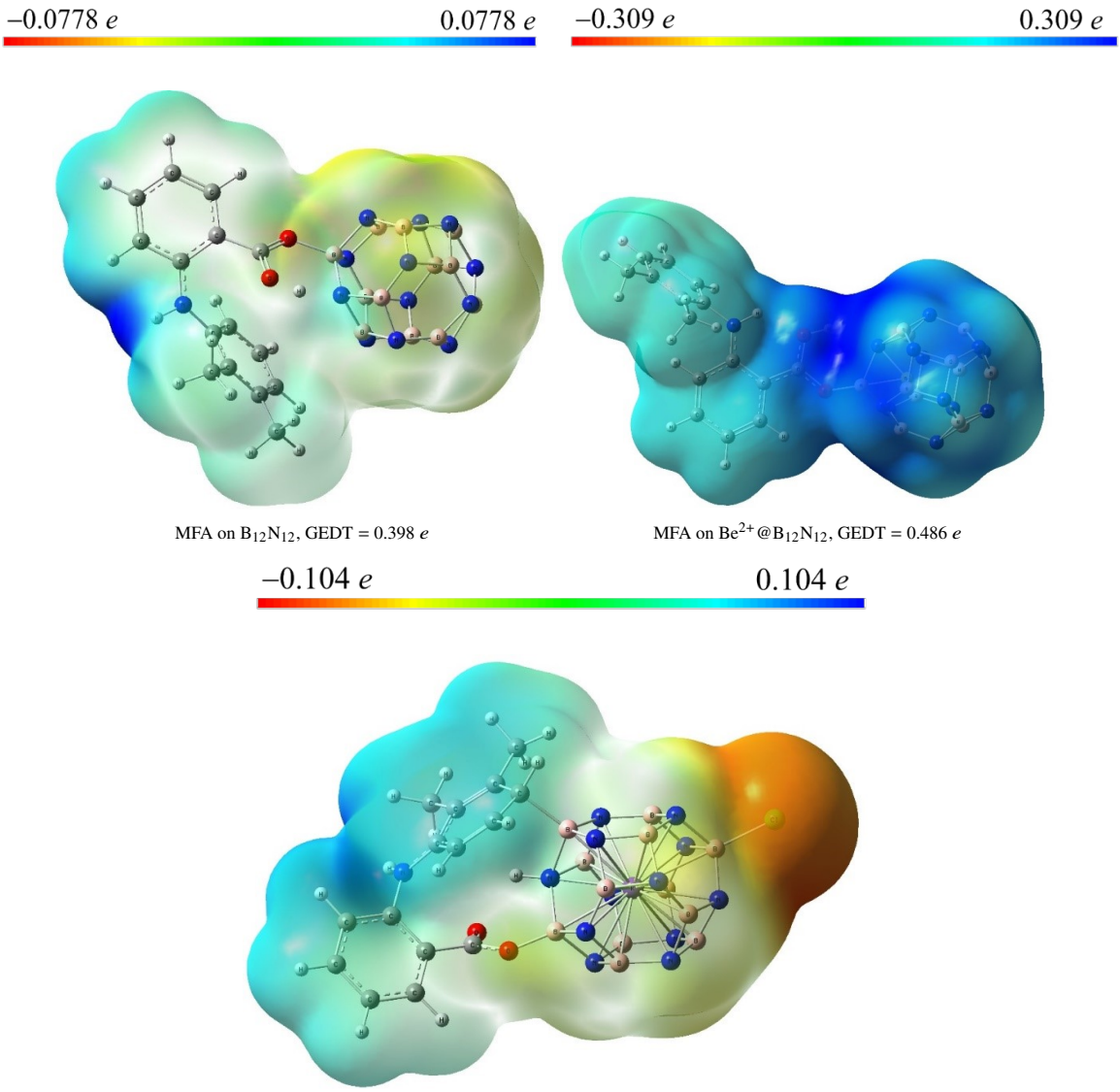

(a) MFA on $K^+@B_{12}N_{12}Cl^-$, GEDT = 0.287 *e*

Figure 8. Molecular electrostatic potential map along with the GEDT values for the most favorable adsorption situation of mefenamic acid on pristine $B_{12}N_{12}$, $Be^{2+}@B_{12}N_{12}$, and $K^+@B_{12}N_{12}Cl^-$ nanocages.

https://doi.org/10.57647/ijnd.2026.1703.04

Figure 9 Electron Localization Function (ELF) analysis for the adsorption complexes of MFA on (a and d) the pristine $B_{12}N_{12}$ nanocage, (b and e) the $Be^{2+}@B_{12}N_{12}$ nanocage, and (c and f) the $K^{+}@B_{12}N_{12}Cl^{-}$ nanocage. The left images (a-c) show color-filled maps of the ELF values on the electron density isosurface, where red indicates regions of highly localized electron pairs (ELF ~ 1), blue specifies complete electron delocalization (ELF ~ 0), and green/yellow regions represents intermediate values. The right images (d-f) depict the corresponding valence attractor positions (basins where electrons are most localized) and their populations (values in red, given in electrons). The high ELF values (red regions) and the presence of strong attractors with significant electron populations between the oxygen atoms of MFA and the boron atom of nanocage provide unequivocal evidence of strong, localized chemical interactions.

The ELF analysis provides evidence of covalent bond

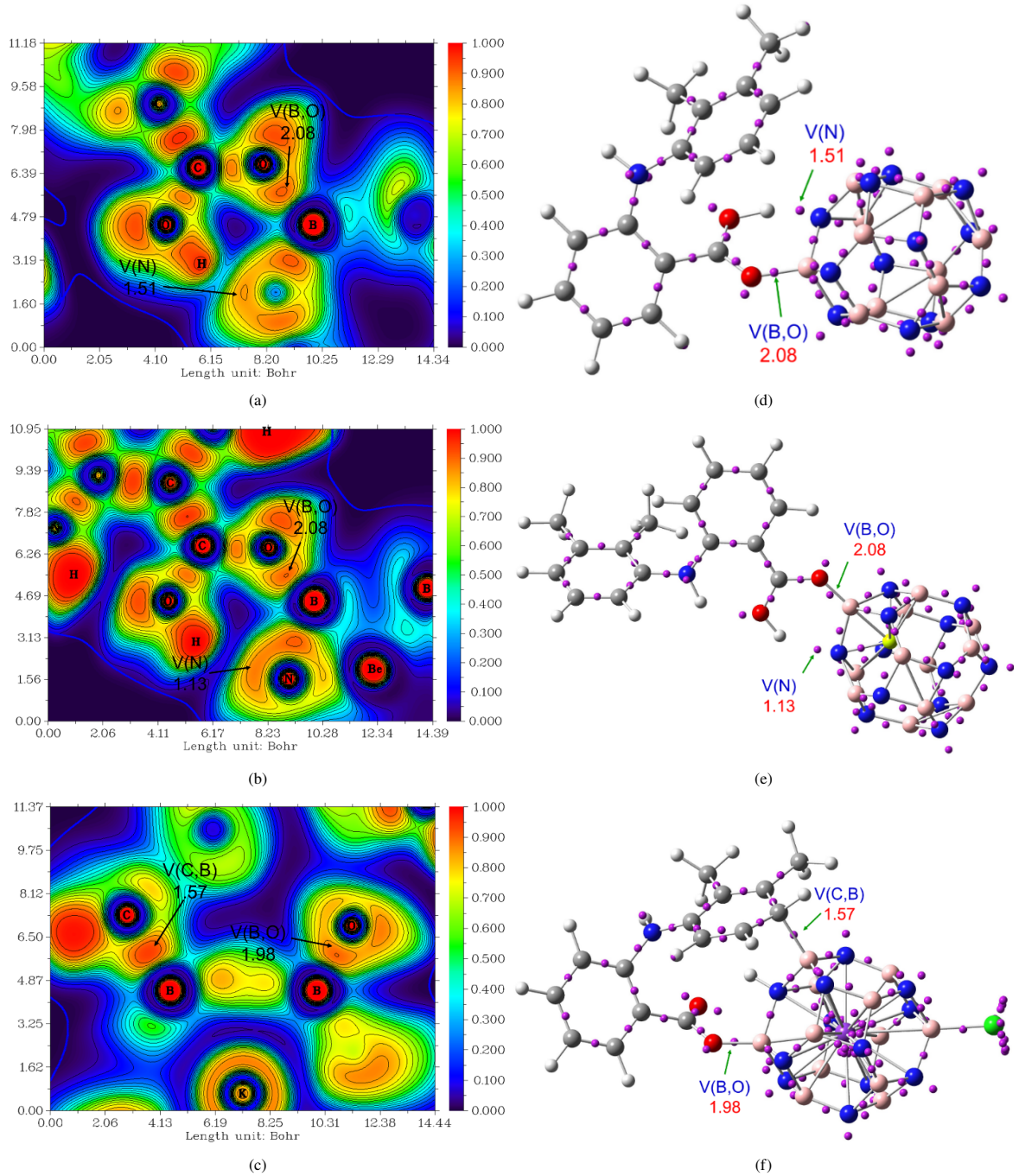

Figure 9. Electron Localization Function (ELF) analysis for the adsorption complexes of MFA on (a and d) the pristine $B_{12}N_{12}$ nanocage, (b and e) the $Be^{2+}@B_{12}N_{12}$ nanocage, and (c and f) the $K^{+}@B_{12}N_{12}Cl^{-}$ nanocage. The left images (a-c) show color-filled maps of the ELF values on the electron density isosurface, where red indicates regions of highly localized electron pairs (ELF ~ 1), blue specifies complete electron delocalization (ELF ~ 0), and green/yellow regions represents intermediate values. The right images (d-f) depict the corresponding valence attractor positions (basins where electrons are most localized) and their populations (values in red, given in electrons). The high ELF values (red regions) and the presence of strong attractors with significant electron populations between the oxygen atoms of MFA and the boron atom of nanocage provide unequivocal evidence of strong, localized chemical interactions.

https://doi.org/10.57647/ijnd.2026.1703.04

formation between MFA and all studied nanocages, definitively confirming the chemical character of adsorption. The quantitative results are summarized as follows:

(1) For the pristine $B_{12}N_{12}$ nanocage, the ELF topology (Figs. 9 (a,d)) exhibites a disynaptic basin with an electron density value of 2.08 *e* between the oxygen atom of the drug and a boron atom of the nanocage. This value is an evidence for the formation of a single covalent B-O bond between the species. Furthermore, a monosynaptic basin with electron density of 1.51 *e* is localized over a nitrogen atom of the nanocage, confirming an N. . .H interaction with MFA.

(2) For the $Be^{2+}@B_{12}N_{12}$ complex (Figs. 9 (b,e)), the covalent character of the B-O bond is resulted, as evidenced by a population of 2.08 *e* in the corresponding disynaptic basin. The electron density at the monosynaptic basin associated with the N. . .H region is calculated to be 1.13 *e*, indicating a slight modification in the interaction strength compared to the pristine cage.

(3) For the $K^+@B_{12}N_{12}Cl^-$ system (Figs. 9 (c,f)), two distinct disynaptic basins are identified, confirming a dual covalent attachment mechanism: the B-O bond with a population of 1.98 *e*, and the B-C bond (between the 4-position carbon atom of phenyl ring and boron atom) with an electron population of 1.57 *e*. Both values are characteristic of single covalent bonds, providing chemical character of the adsorption process.

In conclusion, the ELF analysis quantitatively and topologically supports covalent bond formation. The calculated electron density values within the synaptic basins provide a definitive criterion for the chemical nature of the adsorption. These results, when combined with the IGMH analyses, suggest a complete interpretation for the adsorption process observed in these systems, directly addressing the interests of researchers focused on electronic structure descriptors.

The specific adsorption properties presented in this work highlight the material's considerable potential for practical utilization. Given the extensive recent interest in fullerene and fullerene-like systems, particularly boron nitride nanocages, for drug delivery and sensing platforms, our findings provide a fundamental background for such advancements. The strong and spontaneous interactions observed between MFA and the $Be^{2+}@B_{12}N_{12}$ and $K^+@B_{12}N_{12}Cl^-$ nanocages, especially their stability in aqueous environments, position these systems as potential candidates for nanocarrier design. The significant charge transfer and high adsorption energetics can be employed not only for drug delivery but also for sensing applications, where the adsorption process sends out a detectable electrochemical or optical signal. While further experimental validation is necessary, this theoretical study provides a background for exploring these nanocages as next-generation therapeutic or diagnostic platforms.

While our computational results reveal the remarkable adsorption capabilities of metal-centered $B_{12}N_{12}$ nanocages, several practical considerations and environmental implications must be considered. The potential toxicity of beryllium-based nanomaterials raises significant concerns for environmental applications. Furthermore, the scalability of synthesizing these specific nanocages with certain metal incorporation remains challenging. For practical wastewater treatment, future research should focus on: (1) exploring less toxic alternative metal ion centers (e.g., K^+, Mg^{2+}, or Ca^{2+}) that can provide a better balance between performance and environmental safety; (2) experimental validation of these computational predictions through controlled laboratory studies; (3) studying the stability and potential leaching of metal ions from the nanocages in various aqueous sources; and (4) developing the processes to prevent the release of these nanomaterials into environment. Such studies would be necessary for translating these computational outcomes into practical and environmentally safe applications.

4. Conclusion

One fundamental human concern is the removal of pharmaceutical pollutants from surface waters to prevent damage to ecosystems. Thus, numerous experimental and theoretical investigations have been carried out on the application of nanomaterials for the treatment of surface water to address this concern. This theoretical study investigates the adsorption of mefenamic acid (MFA) drug on pristine $B_{12}N_{12}$ nanocage and metal-ion-centered nanocages (with alkali and alkaline earth metals) as adsorbents. Various adsorption configurations of MFA on $B_{12}N_{12}$ and metal-centered nanocages in both gaseous and solution phases revealed that the adsorption process is generally exothermic. The strongest adsorption of MFA on $B_{12}N_{12}$ occurs via the interaction between the carboxyl oxygen of MFA and a boron atom of the nanocage. For metal-centered nanocages, when Be^{2+} is located in the center of the nanocage ($Be^{2+}@B_{12}N_{12}$), the adsorption energy has been increased dramatically, resulting in strong adsorption. In addition, in the neutral state, MFA adsorption on $K^+@B_{12}N_{12}Cl^-$ yielded optimal results. Among all structures studied in this work, the last nanocage ($K^+@B_{12}N_{12}Cl^-$) provided the best results in aqueous solution. IGMH analysis revealed that in the most favorable adsorption configuration on $B_{12}N_{12}$, a blue-colored isosurface is observed between MFA and the nanocage, indicating significant intermolecular interactions. The IGMH and NCI analyses further confirmed strong adsorption for both Be^{2+}-centered and $K^+@B_{12}N_{12}Cl^-$ nanocages with MFA. Charge transfer studies demonstrated that mefenamic acid acts as an electron donor while the nanocage plays the role of an electron acceptor. ELF analysis confirmed the formation of strong single bonds between MFA and the nanocage in all optimized adsorption configurations. Overall, this

https://doi.org/10.57647/ijnd.2026.1703.04

work establishes ion encapsulation as a highly effective strategy for engineering the adsorption properties of boron nitride nanocages. The noticeable finding of this work is the remarkably performance of $Be^{2+}@B_{12}N_{12}$ and $K^{+}@B_{12}N_{12}Cl^{-}$ relative to their pristine structure. This finding demonstrates a significant advancement over previous studies on BN nanocage adsorbents, which primarily focused on single metal dopants. In contrast to the earlier work, our research systematically demonstrates how the strategic selection of specific metal ions can significantly enhance adsorption performance. This work opens a novel and versatile route for engineering boron nitride nanomaterials to remove specific pharmaceutical pollutants with high yield.

Acknowledgment
This work was made possible through financial support from the Biosensor and Energy Research Center, Ayatollah Boroujerdi University.

Authors contributions
All authors contributed equally to the conception, design, execution, and writing of this work. All authors read and approved the final manuscript.

Availability of data and materials
The authors declare that the data supporting the findings of this study are available within the paper.

Conflict of interests
The authors assert that they do not have any identifiable conflicting financial interests or personal relationships that might be perceived to influence the work presented in this paper.

References

1. Ahmed M and Hameed B. "Removal of emerging pharmaceutical contaminants by adsorption in a fixed-bed column: a review. " Ecotoxicol. Environ. Saf. 2018; 149:257–66. DOI: 10.1016/j.ecoenv.2017.12.012
2. Feng L, van Hullebusch ED, Rodrigo MA, Esposito G, and Oturan MA. "Removal of residual anti-inflammatory and analgesic pharmaceuticals from aqueous systems by electrochemical advanced oxidation processes. A review. " Chem. Eng. J. 2013; 228:944–64. DOI: 10.1016/j.cej.2013.05.061
3. Bakr AR and Rahaman MS. "Crossflow electrochemical filtration for elimination of ibuprofen and bisphenol a from pure and competing electrolytic solution conditions. " J. Hazard. Mater. 2019; 365:615–21. DOI: 10.1016/j.jhazmat.2018.11.015
4. Cimolai N. "The potential and promise of mefenamic acid. " Expert Rev. Clin. Pharmacol. 2013; 6:289–305. DOI: 10.1586/ecp.13.15
5. Araujo L, Villa N, Camargo N, Bustos M, García T, and Prieto ADJ. "Persistence of gemfibrozil, naproxen and mefenamic acid in natural waters." Environ. Chem. Lett. 2011; 9:13–8. DOI: 10.1007/s10311-009-0239-5
6. Fent K, Weston AA, and Caminada D. "Ecotoxicology of human pharmaceuticals." Aquat. Toxicol. 2006; 76:122–59. DOI: 10.1016/j.aquatox.2005.09.009
7. Tauxe-Wuersch A, De Alencastro LF, Grandjean D, and Tarradellas J. "Occurrence of several acidic drugs in sewage treatment plants in Switzerland and risk assessment. " Water Res. 2005; 39:1761–72. DOI: 10.1016/j.watres.2005.03.003
8. Vaziri I, Amini I, Poor Heravi MR, and Rzayev R. "A density functional theory study of adsorption dimethyl fumarate on the surface of the pristine of g-C3N4 and Fe, Ni and Cu decorated graphitic carbon nitride. " Chemical Review and Letters 2025; 8:52–67. DOI: 10.22034/crl.2024.454286.1327
9. Behjatmanesh-Ardakani R and Rzayev R. "Hydrogen assisted SO_2 dissociation on the Pt-doped graphene quantum dot surface: a non-periodic DFT study. " Chemical Review and Letters 2025; 8:178–86. DOI: 10.22034/crl.2024.489135.1476
10. Ghnim ZS, Adthab AH, Mahdi MS, Mansoor AS, Radi UK, Abd NS, and Kareem RO. "Enhanced adsorption performance and efficiency of graphitic GaN monolayers through functionalizing with transition metal adatoms (Co, Cu and Ni): A DFT study." Chemical Review and Letters 2024; 7:912–25. DOI: 10.22034/crl.2024.467458.1375
11. Ali Q, Shakoor A, Rehman G, Ur Rehman M, Khan M, Ahmad R, Ahmad I, AlAsmari AF, and Alasmari F. "Assessment of the potential and application of $Be_{12}O_{12}$ nanocage for removal of ciprofloxacin from water employing density functional theory." Scientific Reports 2025; 15:1020. DOI: 10.1038/s41598-025-85155-3
12. Gul S, Kainat, Ali Q, Khan M, Ur Rehman M, AlAsmari AF, Alasmari F, and Alharbi M. "Exploring the promising application of $Be_{12}O_{12}$ nanocage for the abatement of paracetamol using DFT simulations." Scientific Reports 2023; 13:18481. DOI: 10.1038/s41598-023-45674-3
13. Soleymani M, Dashti Khavidaki H, and Yarahmadi H. "The Interaction of Sulfamethoxazole Drug with the Pristine and Functionalized C60 Fullerenes: A DFT Study." Phys. Chem. Res. 2024; 12:1079–90. DOI: 10.22036/pcr.2024.458030.2528
14. Soleymani M and Khavidaki HD. "Inactivation possibility of pyrene by C20 fullerene via cycloaddition reactions: A theoretical study. " Comput. Theor. Chem. 2017; 1112:37–45. DOI: 10.1016/j.comptc.2017.04.014

15. Saadh MJ, Hsu CY, Kareem RA, Jafarova AM, Zareii A, Edalat M, and Mirzaei M. "Computational assessments of 5-Fluorocytosine (Flucytosine) antifungal adsorption onto a fullerene oxide nanocage for engineering a potential drug delivery platform. " Chemical Review and Letters 2025; 8:547–54. DOI: 10.22034/crl.2025.512441.1561

16. Dashti Khavidaki H and Soleymani M. "A DFT Study on Adsorption of Alanine on Pristine, Functionalized and Boron and/or Nitrogen Doped Functionalized C60 Fullerenes. " Phys. Chem. Res. 2020; 8:657–69. DOI: 10.22036/PCR.2020.227279.1759

17. Jensen F and Toftlund H. "Structure and stability of C24 and $B_{12}N_{12}$ isomers. " 1993; Chem. Phys. Lett.:89–96. DOI: 10.1016/0009-2614(93)85039-Q

18. Roy S, Zhang X, Puthirath AB, Meiyazhagan A, Bhattacharyya S, Rahman MM, Babu G, Susarla S, Saju SK, and Tran MK. "Structure, properties and applications of two-dimensional hexagonal boron nitride. " Adv. Mater. 2021; 33:2101589. DOI: 10.1002/adma.202101589

19. Moon S, Kim J, Park J, Im S, Kim J, Hwang I, and Kim JK. "Hexagonal boron nitride for next-generation photonics and electronics. " Adv. Mater. 2023; 35:2204161. DOI: 10.1002/adma.202204161

20. Kaviani S, Shahab S, and Sheikhi M. "Adsorption of alprazolam drug on the $B_{12}N_{12}$ and $Al_{12}N_{12}$ nano-cages for biological applications: A DFT study." Physica E: Low Dimens. Syst. Nanostruct. 2021; 126:114473. DOI: 10.1016/j.physe.2020.114473

21. Khavidaki HD, Soleymani M, and Shirzadi S. "A DFT study on adsorption of diazinon and fenitrothion on nanocages $B_{12}N_{12}$ and $B_{12}P_{12}$. " Struct. Chem. 2014; 34:1133–42. DOI: 10.1007/s11224-022-02062-3

22. Strout DL. "Structure and stability of boron nitrides: isomers of $B_{12}N_{12}$. " J. Phys. Chem. A 2000; 104:3364–6. DOI: 10.1021/jp994129a

23. Li W, Jiang L, Jiang W, Wu Y, Guo X, Li Z, Yuan H, and Luo M. "Recent advances of boron nitride nanosheets in hydrogen storage application." J. Mater. Res. Technol. 2023; 26:2028–42. DOI: 10.1016/j.jmrt.2023.08.035

24. Kainat, Gul S, Ali Q, Khan M, Rehman MU, Ibrahim M, AlAsmari AF, Alasmari F, and Alharbi M. "Theoretical modeling of $B_{12}N_{12}$ nanocage for the effective removal of paracetamol from drinking water. " Computation 2023; 11:183. DOI: 10.3390/computation11090183

25. García-Laiton G, Lopez FAZ, Shakerzadeh E, and Chigo-Anota E. "Role of homonuclear B–B/N–N bonds in DNA nucleobases adsorption on boron nitride fullerenes: Biosensor and drug transport implications. " Comput. Theor. Chem. 2025; 1248:115188. DOI: 10.1016/j.comptc.2025.115188

26. Bautista MF, Conde JG, Juárez AR, and Anota EC. "$B_{12}N_{12}$ structures (pristine, isomer and doped with carbon) for drug delivery: The case of the acetylsalicylic acid." Nano Express 2025; 6:015015. DOI: 10.1088/2632-959X/adb988

27. Chantes-Daza M, Salvador NB, Laiton GG, Villanueva MS, and Anota EC. "Is it possible to protect nitric oxide by the $B_{36}N_{36}$ structure?: An in-silico proposal. " Comput. Theor. Chem. 2025 :115448. DOI: 10.1016/j.comptc.2025.115448

28. Ammar H, Badran H, and Eid KM. "TM-doped $B_{12}N_{12}$ nano-cage (TM= Mn, Fe) as a sensor for CO, NO, and NH_3 gases: A DFT and TD-DFT study. " Mater. Today Commun. 2020; 25:101681. DOI: 10.1016/j.mtcomm.2020.101681

29. Baei MT, Bagheri Z, and Peyghan AA. "Transition metal atom adsorptions on a boron nitride nanocage. " Struct. Chem. 2013; 24:1039–44. DOI: 10.1007/s11224-012-0132-x

30. Abbasi M, Nemati-Kande E, and Mohammadi MD. "Doping of the first row transition metals onto $B_{12}N_{12}$ nanocage: A DFT study." Comput. Theor. Chem. 1132

31. Beheshtian J, Tabar MB, Bagheri Z, and Peyghan AA. "Exohedral and endohedral adsorption of alkaline earth cations in BN nanocluster." J. Mol. Model. 2013; 19:1445–50. DOI: 10.1007/s00894-012-1702-y

32. Janjua MRSA. "Theoretical framework for encapsulation of inorganic $B_{12}N_{12}$ nanoclusters with alkaline earth metals for efficient hydrogen adsorption: a step forward toward hydrogen storage materials." Inorg. Chem. 2021; 60:2816–28. DOI: 10.1021/acs.inorgchem.0c03730

33. Janjua MRSA. "Prediction and understanding: Quantum chemical framework of transition metals enclosed in a $B_{12}N_{12}$ inorganic nanocluster for adsorption and removal of DDT from the environment. " Inorg. Chem. 2021; 60:10837–47. DOI: 10.1021/acs.inorgchem.1c01760

34. Ali Q, Khan AA, Yar M, Khan M, Ahmad R, and Ahmad I. "Theoretical insight of ciprofloxacin removal from water using boron nitride ($B_{12}N_{12}$) nanocage". Surf. Interf. 2022; 31:101982. DOI: 10.1016/j.surfin.2022.101982

35. Sheikhi M, Kaviani S, Azarakhshi F, and Shahab S. "Superalkali X3O (X = Li, Na, K) doped $B_{12}N_{12}$ nano-cages as a new drug delivery platform for chlormethine: A DFT approach." Comput. Theor. Chem. 2022; 1212:113722. DOI: 10.1016/j.comptc.2022.113722

36. Mehboob MY, Hussain R, Younas F, Jamil S, Iqbal MMA, Ayub K, Sultana N, and Janjua MRSA. "Computation assisted design and prediction of alkali-metal-centered $B_{12}N_{12}$ nanoclusters for efficient H2 adsorption: new hydrogen storage ma-

terials." J. Cluster Sci. 2023; 34:1237–47. DOI: 10.1007/s10876-022-02294-7

37. Lai Y, Al-Musawi TJ, Hussein UAR, Waleed I, Ahmed HH, Khallawi AQ, Alsaraf KM, Asiri M, Abosaooda M, and Alsaab HO. "A first-principal study of pure and encapsulation boron nitride cluster with alkaline metals as the metformin drug carrier. " J. Mol. Liq. 2023; 384:122260. DOI: 10.1016/j.molliq.2023.122260
38. Oku T, Nishiwaki A, and Narita I. "Formation and atomic structure of $B_{12}N_{12}$ nanocage clusters studied by mass spectrometry and cluster calculation. ." Science and Technology of Advanced Materials 2004; 5:635–8. DOI: 10.1016/j.stam.2004.03.017
39. Nair RGS, Nair AKN, and Sun S. "Adsorption of drugs on $B_{12}N_{12}$ and $Al_{12}N_{12}$ nanocages." RSC Adv. 2024; 14:31756–67. DOI: 10.1039/D4RA05586A
40. Nasrollahzadeh M, Sajjadi M, Iravani S, and Varma RS. "Green-synthesized nanocatalysts and nanomaterials for water treatment: Current challenges and future perspectives." J. Hazard. Mater. 2021; 401:123401. DOI: 10.1016/j.jhazmat.2020.123401
41. Sanni SE, Oni BA, Okoro EE, and Pandya S. "Recent advances in the use of biogenic nanomaterials and photocatalysts for wastewater treatment: challenges and future prospects. " Frontiers in Nanotechnology 2024; 6:1469309. DOI: 10.3389/fnano.2024.1469309
42. Palani G, Arputhalatha A, Kannan K, Lakkaboyana SK, Hanafiah MM, Kumar V, and Marella RK. "Current trends in the application of nanomaterials for the removal of pollutants from industrial wastewater treatment-a review. " Molecules 2021; 26:2799. DOI: 10.3390/molecules26092799
43. Rath P, Bhardwaj LK, Yadav P, and Bhardwaj AK. "A synthesis of biogenic nanoparticles (NPs) for the treatment of wastewater and its application: A review. " Biogenic Wastes-Enabled Nanomaterial Synthesis: Applications in Environmental Sustainability 2024 :127–48. DOI: 10.1007/978-3-031-59083-2_5
44. Soleymani M, Khavidaki HD, and Hosseini M. "Three-component coupling reaction of the C60 fullerene, indole and propargyl bromide: a theoretical study. " React. Kinet. Mech. Catal. 2020; 130:75–90. DOI: 10.1007/s11144-020-01776-x
45. Soleymani M. "Theoretical Study of the Possibility of Functionalization of C20 Fullerene with the Simplest Ketene CH_2CO. " J. Struct. Chem. 2019; 60:524–35. DOI: 10.1134/S0022476619040036
46. Fekri MH, Bazvand R, Soleymani M, and Mehr MR. "Adsorption of Metronidazole drug on the surface of nano fullerene C60 doped with Si, B and Al: A DFT study. " Int. J. Nano Dimens. 2020; 11:346–54
47. Fekri MH, Bazvand R, Solymani M, and Razavi Mehr M. Phys. Chem. Res. 2021; Adsorption behavior, electronical and thermodynamic properties of ornidazole drug on C60 fullerene doped with Si, B and Al: A quantum mechanical simulation.:151–64. DOI: 10.22036/pcr.2020.244279.1814
48. Zhao Y and Truhlar DG. "Comparative DFT study of van der Waals complexes: rare-gas dimers, alkaline-earth dimers, zinc dimer, and zinc-rare-gas dimers. " J. Phys. Chem. A 2006; 110:5121–9. DOI: 10.1021/jp060231d
49. Reed AE, Weinstock RB, and Weinhold F. "Natural population analysis. " J. Chem. Phys. 1985; 83:73546. DOI: 10.1063/1.449486
50. Frisch M, Trucks G, Schlegel H, Scuseria G, Robb M, Cheeseman J, Scalmani G, Barone V, Mennucci B, and Petersson G. b Gaussian 09, Revision E. 01. Gaussian, Inc., Wallingford, CT, USA.
51. Tomasi J and Persico M. "Molecular interactions in solution: an overview of methods based on continuous distributions of the solvent. " Chem. Rev. 1994; 94:2027–94. DOI: 10.1021/cr00031a013
52. Cances E, Mennucci B, and Tomasi J. "A new integral equation formalism for the polarizable continuum model: Theoretical background and applications to isotropic and anisotropic dielectrics. " J. Chem. Phys. 1997; 107:3032–41. DOI: 10.1063/1.474659
53. Lu T and Chen F. "Multiwfn: a multifunctional wavefunction analyzer. " J. Comput. Chem. 2012; 33:580–92. DOI: 10.1002/jcc.22885
54. Chai JD and Head-Gordon M. "Long-range corrected hybrid density functionals with damped atom–atom dispersion corrections. " Phys. Chem. Chem. Phys. 2008; 10:6615–20. DOI: 10.1039/B810189B
55. Marenich AV, Cramer CJ, and Truhlar DG. "Universal solvation model based on solute electron density and on a continuum model of the solvent defined by the bulk dielectric constant and atomic surface tensions." J. Phys. Chem. B 2009; 113:6378–96. DOI: 10.1021/jp810292n
56. Lefebvre C, Rubez G, Khartabil H, Boisson JC, Contreras-García J, and Henon E. "Accurately extracting the signature of intermolecular interactions present in the NCI plot of the reduced density gradient versus electron density." Phys. Chem. Chem. Phys. 2017; 19:17928–36. DOI: 10.1039/C7CP02110K
57. Lu T and Chen Q. " Independent gradient model based on Hirshfeld partition: A new method for visual study of interactions in chemical systems. " J. Comput. Chem. 2022; 43:539–55. DOI: 10.1002/jcc.26812

58. Johnson ER, Keinan S, Mori-Sánchez P, Contreras-García J, Cohen AJ, and Yang W. “Revealing noncovalent interactions. ” J. Am. Chem. Soc. 2010; 132:6498–506. DOI: 10.1021/ja100936w

59. Domingo LR. “A new C–C bond formation model based on the quantum chemical topology of electron density. ” RSC Adv. 2014; 4:32415–28. DOI: 10.1039/C4RA04280H